An orthogonal projection and regularization technique for magnetospheric radio tomography

Yuhu Zhai[1] and Steven A. Cummer[1]

Received 1 February 2005; revised 10 November 2005; accepted 18 November 2005; published 10 March 2006.

[1] A challenging problem in ill-posed inverse problems is incorporating prior knowledge of the solution into reconstruction techniques. This problem is particularly important in magnetospheric radio tomography where the path integrated measurements of the target region may be sparse. We present in this paper an orthogonal projection and regularization (OPR) technique that incorporates prior knowledge of magnetospheric parameters from existing models or past measurements into a direct reconstruction algorithm. The OPR scheme extracts first an optimal orthonormal basis containing the main features of the unknowns from an ensemble of modeled or measured snapshots through the proper orthogonal decomposition (POD) and then projects the line-of-sight equations onto the subspace spanned by the empirical orthonormal basis. The resulting low-dimensional model is well-conditioned, its coordinates are uncorrelated, and it contains prior knowledge of the solution. The magnetospheric parameters in the transformed coordinate are reconstructed from the low-dimensional model and quantities in the physical coordinate are easily recovered from the POD transformation. On the basis of magnetohydrodynamic (MHD) simulations and hypothetical satellite constellations, we demonstrate that the POD-based method may perform significantly better than the regularized direct method with sparse path-integrated measurements, combined with a few (5–10) model snapshots.

Citation: Zhai, Y., and S. A. Cummer (2006), An orthogonal projection and regularization technique for magnetospheric radio tomography, *J. Geophys. Res.*, *111*, A03207, doi:10.1029/2005JA011039.

1. Introduction

[2] Radio tomography was introduced by *Austen et al.* [1988] and has since been successfully used for the characterization of ionospheric structure [*Fougere*, 1995; *Walker et al.*, 1996; *Sutton and Na*, 1996; *Kamalabadi et al.*, 1999] by integrated line-of-sight measurements. Radio tomography has recently been shown to be a promising new technique for large-scale remote sensing of Earth's magnetosphere in theoretical studies with magnetohydrodynamic (MHD) simulations [*Ergun et al.*, 2000; *Ganguly et al.*, 2000; *Zhai and Cummer*, 2005], as well as in satellite radio propagation experiments [*Cummer et al.*, 2001; *Cummer et al.*, 2003]. The ability to accurately image both the electron density and the magnetic field on a large scale from a few simultaneous measurements of phase difference (or group delay) and Faraday rotation of two coherent radio signals would be a major advance for magnetospheric science to address many currently unanswered fundamental questions [*Ergun et al.*, 2000].

[3] Although currently no magnetospheric tomography satellites exist or are planned, a series of successful radio propagation experiments with IMAGE, WIND, and CLUSTER spacecraft clearly showed that multiple satellites could effectively receive signals from a single transmitter [*Cummer et al.*, 2003], as would be needed in a dedicated magnetospheric radio tomography mission. The unique capability of IMAGE to CLUSTER radio transmissions is the instantaneous multipath measurements due to the four CLUSTER spacecraft. The large spacecraft separations provide opportunities of limited but genuine multipath tomographic reconstruction in large volume of Earth's magnetosphere. On the basis of hypothetical satellite constellations with sparse path-integrated measurements, we introduced a regularized direct method for magnetospheric radio tomography [*Zhai and Cummer*, 2005]. We demonstrated that the regularized direct method performs significantly better compared to the iterative methods when fewer than 10 satellites are available for path-integrated measurements, and it is robust and flexible for a reasonably accurate reconstruction in different regions of the Earth's magnetosphere. The performance of this method, however, may degrade considerably with increasing sparsity of the measurements as maybe limited by practical constraints of satellite missions such as the IMAGE and CLUSTER experiments the measurement behind radio tomography and thus validating the concept of magnetospheric radio tomography. It is advantageous therefore for existing reconstruction techniques to incorporate as much as possible additional

[1]Electrical and Computer Engineering Department, Duke University, Durham, North Carolina, USA.

0148-0227/06/2005JA011039$09.00

information of the magnetospheric parameters that may be available from past measurements or MHD models. The inclusion of prior knowledge of the unknown parameters in tomography may greatly improve the reconstruction. It has been shown in ionospheric tomography that accounting for statistical knowledge of the probed region can make reconstructions much more robust in the presence of noise and highly underdetermined measurements [*Kamalabadi et al.*, 1999]. Many standard approaches, like those studied by *Ganguly et al.* [2000] and *Ergun et al.* [2000], have no provision for including this potentially valuable information.

[4] Additional information in the prior knowledge is useful because it contains the main characteristics of the unknowns, e.g., the empirical model parameters are extracted from a variety of past measurements or MHD simulations in different situations, therefore they produce fields that are statistically similar to target fields. A radio tomography technique that combines the line-of-sight measurements and prior knowledge of the unknown parameters has not been developed in previous research; its scientific interests and practical needs are, however, significant and compelling. An important question is, how to incorporate all useful information inherited in the empirical models or past measurements of the unknowns into existing reconstruction algorithms? Specifically, for an accurate target or boundary detection such as bow shock location in Earth's magnetosphere, we expect the bow shock to be a relatively sharp boundary between two different plasma populations, and the boundary location of bow shock is known statistically, together with roughly its shape and statistical distribution. The challenge is how to use this information, in addition to the path-integrated measurements, to detect the boundary location and thus improve tomography reconstruction, particularly for sparse constellation with very few path-integrated noisy measurements?

[5] Depending on the irregular structures in the probed region in the magnetosphere, radio tomographic problems can be divided into deterministic and statistical ones. For deterministic problems, the structure of some large-scale irregularities or group of irregularities is to be constructed. For statistical problems, in which a great number of irregularities are in the probed region, the statistical parameters of irregularities such as the correlation function of electron density or magnetic field fluctuations are to be constructed [*Kunitsyn and Tereshchenko*, 2003]. Our interest here is to incorporate prior knowledge of the solution into a direct reconstruction when solving the deterministic problem, which is distinct from the statistical radio tomographic problems.

[6] In this paper our primary goal is to develop and demonstrate an orthogonal projection and regularization (OPR) technique that combines the path-integrated measurements and prior knowledge of the unknowns in the probed region from MHD simulations. Specifically, the proper orthogonal decomposition (POD) [*Holmes et al.*, 1996] or principal component analysis (PCA) [*Moore*, 1981] is first applied to extract dominant features or coherent structures in the form of empirical basis from the MHD model snapshots, the line-of-sight equations for a direct reconstruction are then projected onto the subspaces spanned by the set of orthonormal basis vectors to obtain a low-dimensional model that best represents these equations. The magnetospheric parameters in the transformed space are tomographically reconstructed from the reduced-order system, and the original parameters in the physical space are easily recovered. Related approaches incorporating a priori information from models for ionospheric radio tomography have been described by *Raymund et al.* [1994] and *Sutton and Na* [1996]. In section 2 we discuss the important differences between these approaches and our approach. Examples involving detailed MHD simulations and hypothetical satellite constellations show that the proposed method can perform significantly better than the regularized direct method even with fewer than six satellites, together with a few number of snapshots selected from the MHD models. We also demonstrate that the POD-based method is robust in the presence of modest noise in the path-integrated measurements. More generally, the proposed framework would allow not only model snapshots but also statistical measurements of the unknowns not discussed here to be employed to improve the quality of a direct tomography reconstruction.

2. Magnetospheric Radio Tomography

[7] Tomographic imaging deals with reconstructing an image from path-integrated measurements along different rays passing through the probed region of interest. The information of interest, such as distribution of the electron density is not directly available. Instead, the path-integrated measurements such as the Total Electron Content (TEC) from either the phase difference or group delay of two coherent radio signals can be easily obtained. In practice, however, these measurements are an incomplete sampling of information and corrupted by noise, making tomographic imaging an ill-posed inverse problem [*Zhai and Cummer*, 2005]. For a meaningful reconstruction in magnetospheric radio tomography, it may be necessary to combine the path-integrated measurements with other useful information such as prior knowledge of the unknowns that indicates what the image should look like. We address the issue of how to combine the path-integrated measurements with the prior knowledge based on the proper orthogonal decomposition (POD) used in statistics [*Loève*, 1955], signal processing [*Castrillońand Amaratunga*, 2002], and various engineering applications [*Zhai*, 2003; Y. Zhai and L. Vu-Quoc, Analysis of power magnetic components with nonlinear static hysteresis: Proper orthogonal decomposition and model reduction, submitted to *IEEE Transactions on Computer-Aided Design and Integrated Circuit Systems*, 2006].

[8] Magnetospheric plasma density N_e and the magnetic field **B** are two primary physical parameters of Earth's magnetosphere. Recent experiments [*Cummer et al.*, 2001] successfully measured the Faraday rotation on a magnetospheric transmission, experimentally validating some of the basic magnetospheric radio tomography concepts.

2.1. Phase Difference and Faraday Rotation

[9] To measure path-integrated N_e, each satellite transmits coherently phased pairs of discrete radio frequency signals to be received by all other satellites. The phase difference and group delay provide integrated measurements of elec-

tron density only, while Faraday rotation provides the product of magnetic field **B** and electron density N_e and is thus sensitive to changes in both quantities [*Cummer et al.*, 2001; *Zhai and Cummer*, 2005]. Faraday rotation is the rotation of polarization of a linearly polarized wave as it travels through a magnetized medium like magnetospheric plasma. The phase difference and Faraday rotation difference in cold-plasma approximation, at a fixed time between two signals with frequencies f_1 and f_2 with respect to f_1 are given as [*Zhai and Cummer*, 2005]

$$\Delta\phi = \frac{f_1}{f_2}\phi_2 - \phi_1 = \left(\frac{f_1 e^2}{4\pi\epsilon_0 m_e c}\right)\left(\frac{1}{f_1^2} - \frac{1}{f_2^2}\right)\int_{s=0}^{s=l} N_e ds, \quad (1)$$

$$\Delta F = -\kappa\left(\frac{1}{f_1^2} - \frac{1}{f_2^2}\right)\int_{s=0}^{s=l} N_e B\cos\theta ds, \quad (2)$$

where $\kappa = \dfrac{e^3}{8\pi^2\epsilon_0 \mathrm{cm}_e^2} = 2.36 \times 10^4\ \mathrm{m}^2\ \mathrm{T}^{-1}\ \mathrm{s}^{-2}$ is a constant factor; e, m_e are the electron charge and mass; ϵ_0 is the free space permittivity; c is the speed of light; and B is the magnitude of the magnetic field **B**.

[10] If the region of interest with m rays is divided into n discrete cells, then the phase difference $\Delta\phi_i$ and the Faraday rotation angle ΔF_i measured through ray i in (1) and (2) with $i = 1, \ldots, m$, can be expressed in a discrete form as [*Zhai and Cummer*, 2005]

$$\mathbf{y}_{m\times 1} = \mathbf{A}_{m\times\{n\ or\ 2n\}}\mathbf{x}_{\{n\ or\ 2n\}\times 1}. \quad (3)$$

In general, $m \ll n$. The vector **x** represents the unknown distribution of N_e or the product of N_e and **B** along the propagation paths at certain discrete points in the probing region. The vector **y** represents the phase difference or the Faraday rotation measurements obtained along ray paths. The matrix **A**, which is a discrete version of the line-integral of (1) and (2), has a dimension of m by n or m by $2n$ for the reconstruction of N_e and the product of N_eB, respectively. We thus focus on solving **x** from (3) in a direct method of reconstructing N_e and **B**. See *Zhai and Cummer* [2005] for more details.

2.2. Direct Tomography Algorithm With Regularization

[11] Owing to the ill-conditioning of **A**, equation (3) is typically solved by minimizing a least squares-type functional. *Zhai and Cummer* [2005] formulate the ill-conditioned inverse problem into a constrained and weighted least-squares minimization problem. The minimization of

$$\mathbf{\Gamma}(\mathbf{x}) = \| \mathbf{Ax} - \mathbf{y} \|^2_{\mathbf{S}_y^{-1}} + \lambda_1 \| \mathbf{Hx} \|^2 + \lambda_2 \| \mathbf{x} \|^2_{\mathbf{S}_{mod}^{-1}} \quad (4)$$

will lead to a unique and stable solution for **x**, where $\mathbf{S}_y$ is the noise covariance matrix for the line-of-sight measurements **y**, and $\mathbf{S}_{mod}$ the covariance matrix of any statistical model of the magnetospheric region being probed. We can also assume an independent identically distributed (IID) noise [*Kamalabadi et al.*, 1999], if the noise covariance information is unknown. The $\mathbf{S}_y$ will thus be a constant times the identity matrix and this constant can be absorbed in the regularization parameters. A two-dimensional five-point finite difference approximation of the second-order Laplacian operator was shown by *Zhai and Cummer* [2005] to perform well for a variety of different regions such as the plasmasheet and the bow shock and thus is used throughout this work for matrix **H** with a slight modification on the boundaries.

[12] Although the statistical regularization has been known to be related to the classical Tikhonov regularization [*Demoment*, 1989; *Kamalabadi et al.*, 1999], an efficient and systematic way to estimate the covariance matrix $\mathbf{S}_{mod}$ needed in the reconstruction has not been found in the literature. A typical approach is to assume that the statistical model has an independent identically distribution (IID), which leads $\mathbf{S}_{mod}$ to be a constant times an identity covariance matrix **I** [*Demoment*, 1989]. Depending on the probed region, this approach, however, may perform poorly in magnetospheric radio tomography with sparse observations. In the work of *Kamalabadi et al.* [1999], a statistical framework for ionospheric tomography has been introduced, and a prior statistical model is also taken to be an IID Gaussian function proved to considerably improve reconstruction with noisy data. The regularization parameter λ_2 and the diagonal terms of $\boldsymbol{S}_{mod}$ are estimated based on an empirically obtained average variance of a series of typical model ionospheres.

[13] A simpler approach to include prior knowledge of the values of the unknown parameters into a direct reconstruction is to require solution to be minimally deviated from the average of all snapshots, similar to incorporating the in situ measurements of the unknowns into the reconstruction as in the work of *Zhai and Cummer* [2005]. Unlike the proper orthogonal projection used in (6), where the solution is free to lie anywhere in the subspace spanned by the set of optimal orthonormal basis vectors, this approach, however, enforces the solution to favor a direction representing the statistical expectation, which does not include variations that would be measured and of interest. Therefore some important features in the ensemble of snapshots will be excluded from the reconstruction, particularly for magnetospheric regions with sharp density and field gradient such as bow shock, where the sharp boundary between two different plasma populations will not be accurately reconstructed.

[14] The POD is a procedure for extracting an orthonormal basis for a modal decomposition from an ensemble of signals or images. Among all possible decompositions of a random field, the POD is the most efficient in the sense that for a given number of modes, the projection on the subspace used for reconstructing the random field will on average contain the most energy possible [*Holmes et al.*, 1996]. Unlike other bases such as piecewise linear functions in the finite element method, Fourier series and wavelets in the spectral method, and polynomials in the finite difference method, the proper orthogonal modes (POMs) are directly extracted from the physical properties of the system of interest. Therefore the POMs contain main characteristics of the expected solution. This optimality of POD makes it suitable for incorporating statistical information into the ill-conditioned image reconstruction process, in which the proper orthogonal projection may significantly reduce dimensionality and thus improve conditioning of the inverse problem.

2.3. Orthogonal Projection and Regularization (OPR) Technique

[15] We now formulate the ill-conditioned inverse problem into a low-dimensional but well-conditioned constrained and weighted least-squares minimization problem by an orthogonal projection or a coordinate transformation of the unknowns. Instead of solving a direct minimization problem (4), which can be written as

$$\hat{\mathbf{x}} = \underset{\mathbf{x}}{\operatorname{argmin}} \boldsymbol{\Gamma}(\mathbf{x}) \ ,$$

we incorporate prior knowledge of the unknowns into the minimization process by projecting $\widehat{\mathbf{x}}$ onto the subspace spanned by the snapshots selected from either the magnetohydrodynamic (MHD) models or past measurements. Specifically, we first extract an optimal orthonormal basis from an ensemble of selected snapshots generated by the models or the measurements, then project $\widehat{\mathbf{x}}$ onto the extracted empirical basis to obtain a generally well-conditioned low-dimensional system, and solve the inverse problem of the low-dimensional system. The system solution in the physical coordinate is easily recovered by the POD transformation.

[16] Let $\mathbf{Q} = [\mathbf{q}_1\ \mathbf{q}_2 \ldots \mathbf{q}_p]$ be an ensemble of unknowns such as the electron density or the magnetic field vector components to be reconstructed. More specifically, suppose we are given a set of p snapshots of the unknowns generated from detailed MHD simulations or any statistical models of past measurements in regions such as the bow shock, magnetotail, or central plasma sheet. We perform singular value decomposition (SVD) to the ensemble, which can be viewed as a discrete realization of the POD or PCA of the ensemble, such that

$$\mathbf{Q} = \mathbf{U}\boldsymbol{\Sigma}\mathbf{V}^T, \tag{5}$$

where $\mathbf{U}$, $\mathbf{V}$, and diagonals of $\boldsymbol{\Sigma}$ are the left and right singular vectors and the corresponding singular values, respectively. The POD is essentially nothing but expressing the unknown $\mathbf{x}$ in terms of the empirical orthonormal basis $\mathbf{U}$ as follows:

$$\mathbf{x} = \mathbf{U}\widetilde{\mathbf{x}}, \tag{6}$$

where $\widetilde{\mathbf{x}}$ is the image of unknown $\mathbf{x}$ in the POD transformed coordinate. We then solve the minimization problem (4) in the transformed coordinate $\widehat{\mathbf{x}} = \operatorname{argmin}\ \boldsymbol{\Gamma}\ (\widetilde{\mathbf{x}})$, as expressed below:

$$\| \mathbf{AU}\widetilde{\mathbf{x}} - \mathbf{y} \|^2_{\mathbf{S}_y^{-1}} + \lambda_1 \| \mathbf{HU}\widetilde{\mathbf{x}} \|^2 + \lambda_2 \| \mathbf{U}\widetilde{\mathbf{x}} \|^2_{\mathbf{S}_{mod}^{-1}} \tag{7}$$

by taking the derivative of (7) with respect to $\widetilde{\mathbf{x}}$, and the solution is then obtained from

$$\mathbf{U}^T\left(\mathbf{A}^T\mathbf{S}_y^{-1}\mathbf{A} + \lambda_1\mathbf{H}^T\mathbf{H} + \lambda_2\mathbf{S}_{mod}^{-1}\right)\mathbf{U}\widetilde{\mathbf{x}} = \mathbf{U}^T\left(\mathbf{A}^T\mathbf{S}_y^{-1}\mathbf{y}\right). \tag{8}$$

Let

$$\widetilde{\mathbf{A}} = \mathbf{U}^T\left(\mathbf{A}^T\mathbf{S}_y^{-1}\mathbf{A} + \lambda_1\mathbf{H}^T\mathbf{H} + \lambda_2\mathbf{S}_{mod}^{-1}\right)\mathbf{U}$$

and

$$\widetilde{\mathbf{y}} = \mathbf{U}^T\left(\mathbf{A}^T\mathbf{S}_y^{-1}\mathbf{y}\right);$$

we thus obtain the low-dimensional model solution in the transformed coordinate as

$$\widetilde{\mathbf{x}} = \widetilde{\mathbf{A}}^{-1}\widetilde{\mathbf{y}}.$$

The solution in the physical coordinate is easily recovered from (6).

[17] Extracting the empirical basis from the SVD of the ensemble matrix $\mathbf{Q}$ is more stable and more efficient than solving the eigenvalue problem of its covariance matrix $\mathbf{K} = \mathbf{QQ}^T$ [*Hung and Senturia*, 1999], as is usually done in the principal component analysis in statistical learning [*Hastie et al.*, 2001]; therefore SVD is used in this work. The definition of $\mathbf{K}$ as the covariance matrix is for our convenience. Each snapshot in matrix $\mathbf{Q}$ is a realization of the same random vector. Therefore the left singular matrix of $\mathbf{Q}$ is used for the orthogonal projection. The reader is referred to *Muller et al.* [2004] for a review of SVD and its application for image reconstructions.

[18] We show below that the statistical samples in the ensemble $\mathbf{Q}$ are uncorrelated after the POD coordinate transformation. From (6) and the orthogonality of the empirical basis $\mathbf{U}$, we express the ith sample in $\mathbf{Q}$ in the subspace spanned by the empirical basis as follows:

$$\widetilde{\mathbf{q}}_i = \mathbf{U}^T\mathbf{q}_i = \mathbf{U}^T\mathbf{Q}\mathbf{e}_i,$$

where $\mathbf{e}_i = \{0\ 0 \ldots 1 \ldots 0\}^T$ is the unit vector with 1 on its ith index only. Therefore

$$\widetilde{\mathbf{q}}_i\widetilde{\mathbf{q}}_i^T = \mathbf{U}^T\mathbf{Q}\mathbf{e}_i\mathbf{e}_i^T\mathbf{Q}^T\mathbf{U} = \mathbf{U}^T\mathbf{Q}\begin{bmatrix} 0 & 0 & \ldots & \ldots & \ldots \\ \ldots & \ldots & \ldots & \ldots & \ldots \\ \ldots & 0 & 1 & 0 & \ldots \\ \ldots & \ldots & \ldots & \ldots & \ldots \\ \ldots & \ldots & \ldots & 0 & 0 \end{bmatrix}\mathbf{Q}^T\mathbf{U}, \tag{9}$$

from (5) and the orthogonality of the left and right singular vectors, we then obtain

$$\widetilde{\mathbf{q}}_i\widetilde{\mathbf{q}}_i^T = \mathbf{U}^T\mathbf{U}\boldsymbol{\Sigma}\mathbf{V}^T\mathbf{e}_i\mathbf{e}_i^T\mathbf{V}\boldsymbol{\Sigma}\mathbf{U}^T\mathbf{U} = \boldsymbol{\Sigma}\mathbf{V}^T\mathbf{e}_i\mathbf{e}_i^T\mathbf{V}\boldsymbol{\Sigma} = \sigma_i^2, \tag{10}$$

where σ_i is the ith singular value of the snapshot matrix $\mathbf{Q}$. Essentially, (5) provides a compact and optimal description of the data set. The set of correlated variables $\mathbf{q}$ of the image in its physical coordinate in (6) is then transformed into a set of uncorrelated variables $\widetilde{\mathbf{q}}$ of the image in the POD coordinate, with the uncorrelated variables $\widetilde{\mathbf{q}}$ ordered by reducing variability, while retaining as much additional useful information as is possible.

[19] The key of this orthogonal projection-based reconstruction is the reformulation of the minimization problem

(4) via the POD coordinate transformation in (6). The reformulated system equation (7) is then projected onto the subspace spanned by the optimal basis **U**, extracted via the SVD of the statistical ensemble **Q**. The rationale lies in that along these directions, the basis is optimal as it captures more energy per basis vector than any other set of basis vectors. In other words, the coordinate transformation in (6) is, in the least-square sense, the best among all other linear decompositions. A geometrical interpretation of the empirical basis is that they are simply the principal axes of the cloud of p data points **Q** in the n-dimensional vector space [*Holmes et al.*, 1996, p. 90].

[20] The main advantage of this approach is that additional information such as prior knowledge of the unknowns from either estimations based on past measurements or MHD model simulations can be easily included in the direct reconstruction. The end result is a reconstruction that may agree considerably well with both the path-integrated measurements **y** in the range of the ill-posed inverse problem, and the prior knowledge of **x** in the domain of the problem. It is maximally smooth in some sense attributed to the smoothing term $\lambda_1\|\mathbf{HU}\tilde{\mathbf{x}}\|^2$ in (7). This approach has practical scientific interests, since in reality a diverse auxiliary information may have been gathered from past measurements or theoretical studies.

[21] The OPR technique is a combination of the orthogonal decomposition, orthogonal projection, and a deterministic regularization for an efficient direct reconstruction. Although the orthogonal decomposition used in our method is the same as that used by *Sutton and Na* [1996] for extracting an orthonormal basis, the formulation of the residual correction method by *Sutton and Na* [1996] is different from ours. Our method uses the orthogonal projection and regularization to reformulate the ill-conditioned inverse problem into a well-conditioned, low-dimensioned problem by projecting the line-of-sight equations onto the subspace spanned by the empirical orthonormal basis and directly solves the problem reformulated. The residual correction method proposed by *Sutton and Na* [1996], on the other hand, does not use any orthogonal projection and regularization. Instead, it uses a less-efficient subspace iteration to improve conditioning of the inverse problem, and a less-robust matrix pseudo-inverse to ensure computational feasibility of the reformulated problem, which involves a series of submatrices decomposed from the complete matrix **A**. The Gauss-Seidel iterative algorithm is used to improve numerical stability. For the ill-conditioned magnetospheric tomographic imaging, the Gauss-Seidel iterative method used by *Sutton and Na* [1996] may have convergence problem and the iterative method may not converge to a minimum norm least squares solution. Our method is also different from the model-assisted ionospheric tomographic method developed by *Raymund et al.* [1994]. The main advantage of our method is that instead of using directly the model realizations or the snapshots for a non-orthogonal projection as in the work of *Raymund et al.* [1994], we extract an orthonormal basis from the snapshots before the projection. Therefore we significantly improved conditioning of the inverse problem by using the orthonormal basis for the reconstruction.

[22] Although our method is not for discovering new structures in the magnetosphere, the scientific significance of the proposed method lies in that in practical magnetospheric radio tomography, basic measurements of the spatial structure and its temporal variation of the large-scale magnetosphere in a multisatellite mission (4–6 satellites) have not been made before and would drastically improve our limited knowledge of how structures like the bow shock and magnetotail vary in response to external forcing from the solar wind.

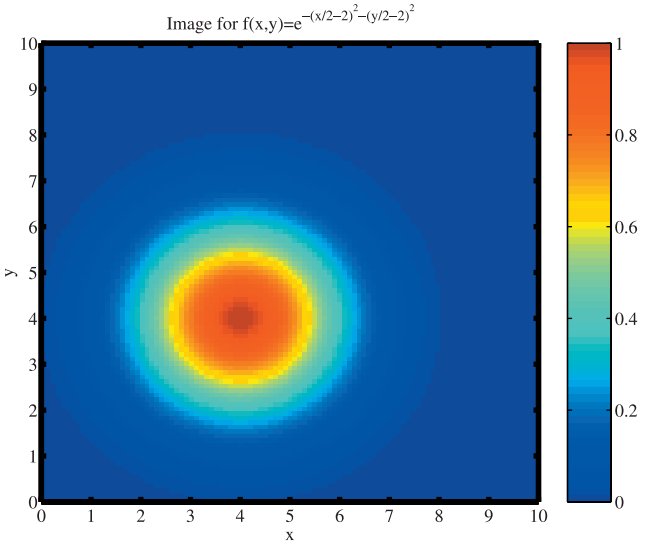

Figure 1. Image of a Gaussian function used in the test problem.

3. Magnetospheric Image Reconstruction

[23] With examples involving two-dimensional images of the plasma density N_e and the magnetic field **B** from detailed MHD simulations of the magnetotail and bow shock of Earth's magnetosphere, we demonstrate performance of the POD-based reconstruction algorithm. The magnetospheric electron density and magnetic field configurations were computed from an MHD simulation [*DeZeeuw et al.*, 2000] available through the Community Coordinated Modeling Center (CCMC) at NASA Goddard Space Flight Center. The electron density is computed from the MHD ion density assuming quasi-neutrality. The probing frequency is selected based on the characteristic physical parameters such as the plasma frequency and electron gyrofrequency of each region of interest in examples in section 3.2.

3.1. Algorithm Validation

[24] A simple test problem is used to validate the proposed method and to compare with the regularized direct method without statistical information [*Zhai and Cummer*, 2005]. The original two-dimensional image of a Gaussian function and its line-of-sight paths are shown in Figure 1 and Figure 2. In addition to the path-integrated measurements, a few snapshot images where the center of the Gaussian function is randomly distributed within the probed region are given from statistical models of the Gaussian function.

[25] Figure 3 shows clearly that the mean-square errors committed by the orthogonal projection-based reconstruction with six and nine snapshots are much smaller than the

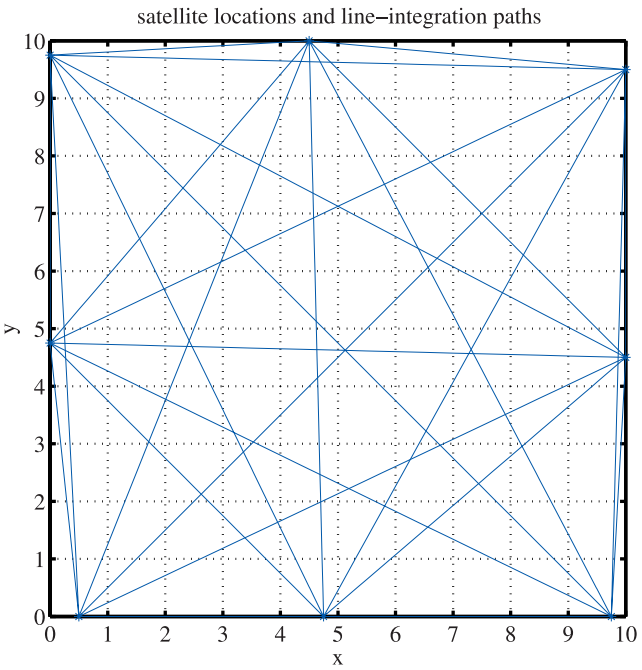

Figure 2. The line-integration paths used in the test problem.

errors committed by the regularized direct reconstruction without a priori information of the Gaussian function. Figure 3 is obtained by reconstructing the image in Figure 1 with center positions of the Gaussian function located along the left-bottom to the right-top diagonal direction in the image, and the snapshots are selected from images with the Gaussian function center randomly distributed along the left-bottom to the right-top diagonal direction. For a more challenging test, the snapshot images are selected to be not too close to the true image. We therefore exclude the possibility of imposing the solution towards any of the snapshots in the reconstruction. A greater improvement can be achieved if the snapshots are closer to the true image to be reconstructed.

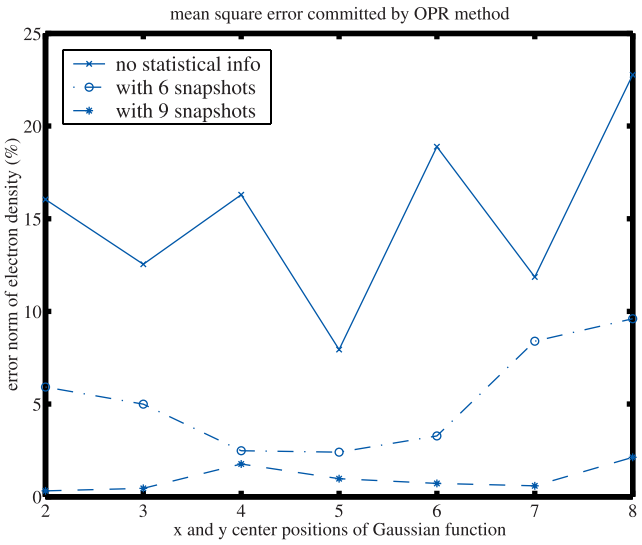

Figure 3. Comparison of reconstruction errors against x and y positions of the Gaussian function center.

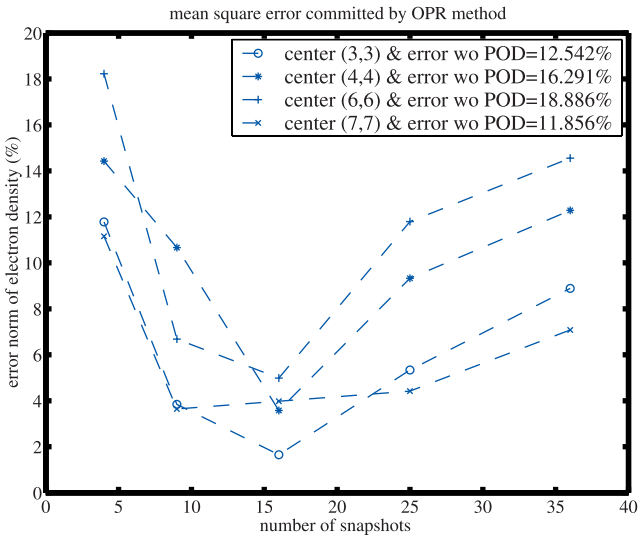

Figure 4. Number of snapshots for reconstructing an image in Figure 1 with eight satellites.

This is attributed to better conditioning of the inverse problem after the orthogonal projection, as well as the incorporation of prior knowledge of the solution contained in the orthonormal basis. Figure 4 is also obtained by reconstructing the image in Figure 1, but the snapshots are selected from images with a Gaussian function center statistically distributed in a two-dimensional subregion in the image plane, instead of a straight line. The Gaussian function center positions of the snapshots are generated from a normal distribution around the center position of the true image with a zero mean and a variance of one. Compared to the regularized direct reconstruction, the better performance of the POD-based reconstruction is mainly attributed to the projection of the unknowns onto the subspace spanned by the set of optimal empirical basis vectors in (6)–(7), which best represent our prior knowledge about the unknowns. The prior knowledge of the solution is thus combined with the line-integral measurements such that a better reconstruction containing the main features of the solution is obtained and a good agreement with the line-integral measurements is achieved.

[26] It is noted in Figure 4 that the number of snapshots employed in the POD has an optimal value, which is between 10 and 25 for the test problem. Below the optimal value, meaning that there are too few snapshots ($\leq$15), the POD-based reconstruction may not achieve any substantial improvement in the mean square errors compared to the regularized direct reconstruction without POD projection as shown in Figure 4 for $\leq$15 snapshots; close to the optimal value (10–25), however, the POD-based reconstruction is significantly better. This is partially due to truncation of the statistical information in the covariance matrix $\mathbf{QQ}^T$ for the orthogonal projection in (7). In other words, we project the reconstruction equation onto a subspace spanned by the covariance matrix. This projection, in the case of too few snapshots, may eliminate some useful information in the path-integrated measurements, thus may introduce undesirable artifacts [*Holmes et al.*, 1996]. On the other hand, consistency of the snapshots with measurements or how far are the snapshots to the

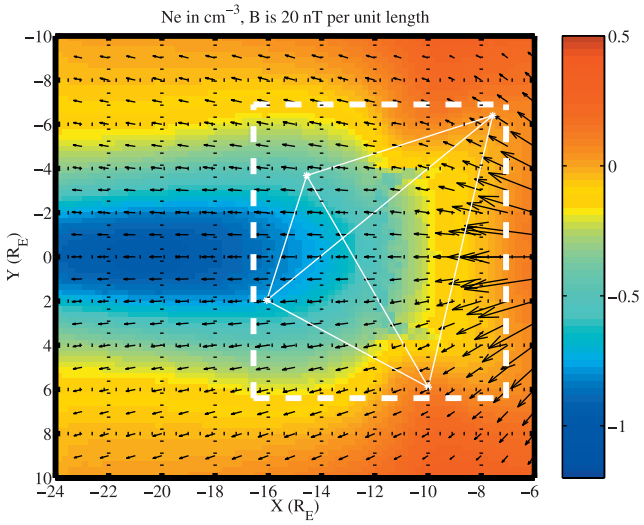

Figure 5. The MHD simulated electron density N_e (logarithm) and magnetic field **B** of the X-Y plane plasma sheet.

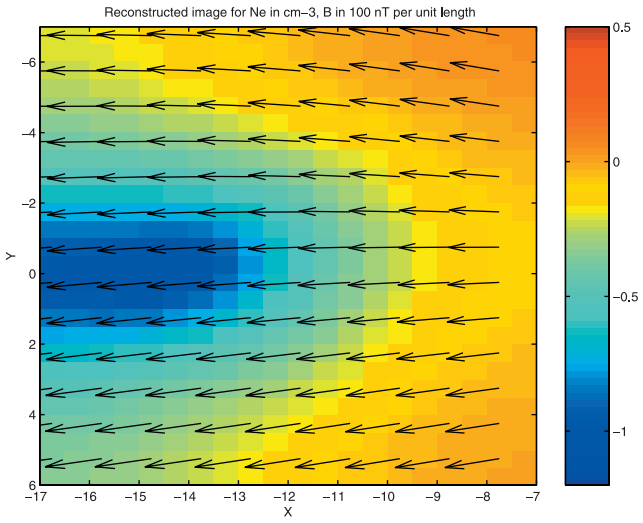

Figure 7. Reconstruction with four satellites from the method without POD projection (11.0%, 36.2% and 75.0% errors in N_e, B_x and B_y respectively).

true image is crucial to the POD-based reconstruction. The larger the distance between the snapshots and the true image, the bigger the reconstruction error, as shown in Figure 4 for >15 snapshots. This is because the snapshots are obtained by randomly selecting the location of the Gaussian function center, adding more snapshots that are too far from the true image may also degrade the POD-based reconstruction. This implies that in situations where few statistical snapshots are available, there is a trade-off between consistency of the snapshots with measurements, i.e., how far are they to the true image, and the number of snapshots used for the POD reconstruction. One strategy for selecting the optimal number of snapshots would be to remove snapshots that seem to be too far from the true image. An effective approach is to compare the line-of-sight projection of each snapshot with the path-integrated measurements. The snapshots whose projections are too far from the true measurements are inconsistent with the data and should not be used. This is similar to the cross validation widely used in statistical model selection literature [*Lin and Pourahadi*, 1998]. The main difference is that magnetospheric tomographic imaging is an ill-conditioned inverse problem with few path-integrated measurements, while the statistical model selection is a well-conditioned but overdetermined problem. Therefore unlike the cross validation used for best-model selection, our method is used for filtering out inconsistent snapshots. The optimal inconsistency threshold is fuzzy and probably problem-dependent. We find empirically that a 100% mean-square error threshold on the electron density measurement works well. Here we treat each measurement as noiseless to explore the maximum potential of tomographic imaging. In practice, however, the path-integrated measurements are noisy and the simple consistency check is used to sort out undesired snapshots.

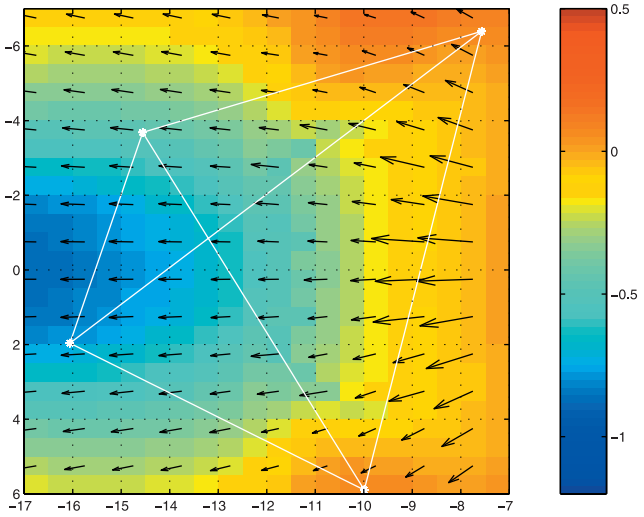

Figure 6. The satellite probed region (right) for an 4-satellite magnetospheric radio tomography mission.

3.2. Performance on Simulated Magnetosphere

[27] The main advantage of the proposed method is its adaptability and extensibility to incorporate a priori information to improve the reconstruction. A priori information could be obtained from either global MHD models or statistical models based on past in situ measurements. A four-satellite imaging of the X-Y plane plasma sheet of the Earth's magnetotail and the satellite probed region are shown in Figure 5 and Figure 6, where brightness scale denotes the electron density and arrow the magnetic field vector. To test performance of the POD-based reconstruction, we use the three-dimensional (3-D) MHD models to generate snapshots to be integrated with the path-integrated measurements. The snapshots were obtained from 3-D MHD simulations at times separated for hours and along different Z planes with a difference of R_Es. Therefore correlations among snapshots are not too tight, since no snapshot is too close to the solution. These snapshots represent our prior knowledge of the unknown image because they provide useful information about what the image should look like. Figure 7 and Figure 8 shows the reconstructed N_e and **B** from the regularized direct method

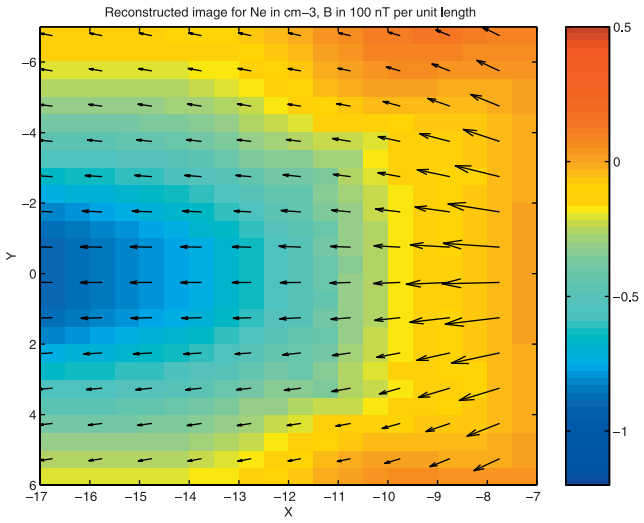

Figure 8. Reconstruction with four satellites from the method with POD projection (2.9%, 14.9% and 16.0% errors in N_e, B_x and B_y, respectively).

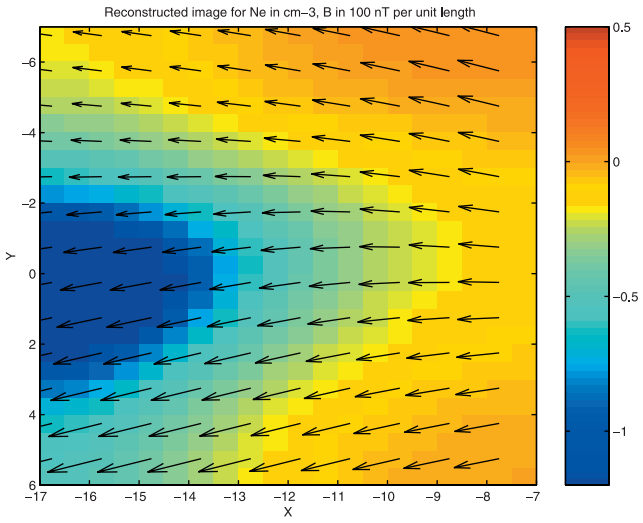

Figure 9. Reconstruction with four satellites from the direct method with 5% WGN (15.9%, 33.5% and 73.2% errors in N_e, B_x and B_y, respectively).

without POD projection and that with the POD projection for the four-satellite tomographic imaging. With the OPR technique, a reconstruction in Figure 8 has 2.9%, 14.9%, and 16.0% mean square errors in N_e, B_x, and B_y, respectively, which is significantly better than the regularized direction reconstruction, where the errors are 11.0%, 36.2%, and 75.0% in N_e, B_x, and B_y, respectively. The **B** reconstruction, particularly the B_y component of **B**, is improved more because the **B** reconstruction by itself is more ill-conditioned, and the optimal POD basis contains the main characteristics of the B_y component. The surprisingly good performance of the direct method without POD projection is mainly attributed to the globally smooth distribution of N_e and **B** in the probed magnetotail region, which is best captured by the smoothing interpolation term $\|\mathbf{Hx}\|^2$ in (4) [*Zhai and Cummer*, 2005]. It is also attributed to the good location of the satellites, whose line-of-sight integration paths can capture most information of the region's magnetospheric parameters. Only six snapshots from the MHD models of the probed region are used for the POD basis extraction. Table 1 shows the distance between each snapshot selected for the POD projection and the true image in terms of mean square error percentages of the reconstructed quantities. It is clear that the best image is extracted from the combination of all snapshots and the path-integrated measurements.

Table 1. Mean Square Error Percentages Between the Selected Snapshots and the True X-Y Plane Magnetotail Image to be Reconstructed[a]

	Snapshot Number					
Parameters	1	2	3	4	5	6
N_e	62.4	25.9	29.8	14.8	11.7	27.5
B_x	46.7	36.9	46.1	37.3	42.9	41.3
B_y	39.4	26.1	38.7	27.0	36.2	31.3

[a]Mean square errors of the POD reconstructed image are 2.9%, 14.9% and 16.0% for N_e, B_x and B_y respectively.

[28] To test performance of the proposed reconstruction method with respect to noise, a 5% White Gaussian Noise (WGN) W with zero mean is added to the measured phase difference and Faraday rotation angle. The WGN is constructed by scaling up a random WGN w by a factor α of 5–10% with respect to the measurement **y**:

$$W = \alpha \mathbf{y} \frac{\mathbf{w}}{\| \mathbf{w} \|}.$$

The magnitude of the WGN is roughly 2 degrees in phase difference measurements, and 0.2 degrees in Faraday rotation measurements. The reconstruction errors of the magnetic field **B** are directly related to the errors of the electron density N_e as discussed by *Zhai and Cummer* [2005]. Figure 9 and Figure 10 show the four-satellite reconstruction in Figure 5

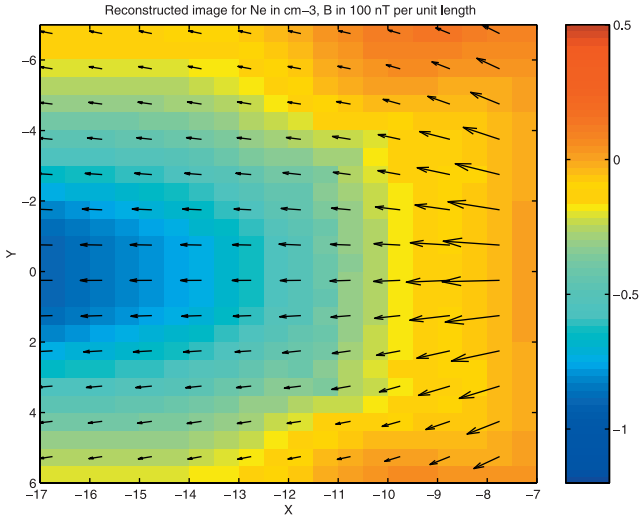

Figure 10. Reconstruction with four satellites from the POD-based method with 5% WGN (4.44%, 20.2% and 17.7% errors in N_e, B_x and B_y, respectively).

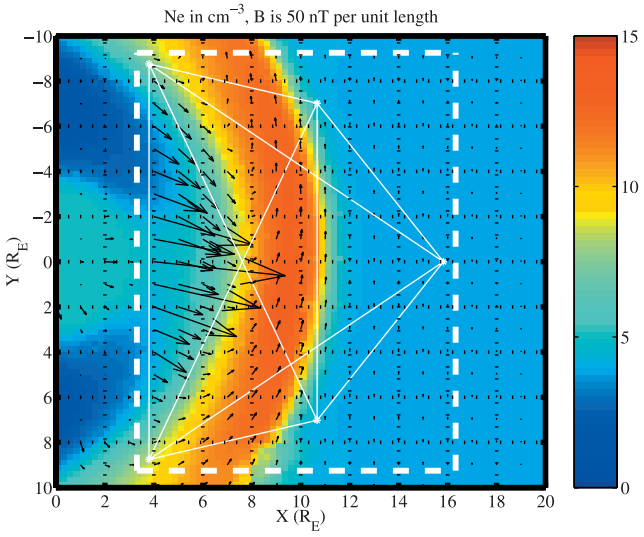

Figure 11. MHD simulated electron density N_e and magnetic field **B**.

by the regularized direct method without POD projection and that with the POD projection. Compared to the reconstruction without POD projection, where the mean square errors are 15.9%, 33.5%, and 73.2% for N_e, B_x, and B_y, respectively, the POD-based method yields a significantly improved reconstruction, with the mean square errors 4.44%, 20.2%, and 17.7% for N_e, B_x, and B_y, respectively. The better performance of the POD-based method is mainly attributed to the inclusion of additional information contained in the snapshots. The POD projection can be viewed as a filtering process that retains the main features of the image reconstructed by the regularized direct method but leaves out any insignificant mismatches of the prior models with the path-integrated measurements. Thanks to the optimal POD basis, which captures quite well the less dominant B_y component of the magnetic field that cannot be characterized by the regularized direct method, a greater improvement in the reconstruction of

Table 2. Mean Square Errors Committed by Direct Method With Deterministic Regularization and the POD-Based OPR Method

Reconstruction Methods	Reconstruction Quantities		
	N_e	B_x	B_y
Regularized direct method	23.7%	154%	123%
OPR method (six snapshots)	16.1%	84.3%	42.1%
OPR method (eight snapshots)	6.65%	28.2%	24.9%

the B_y component is achieved. We therefore demonstrate that the proposed method is more robust in the presence of modest noise, compared with the direct method without the POD projection.

[29] The OPR technique performs particularly well in the magnetospheric regions where sharp density gradient and turbulent magnetic field distribution exist. The bow shock of the Earth's magnetosphere is characterized by an increase in plasma density and increased magnetic field turbulence. It is challenging for conventional direct or iterative algebraic reconstruction techniques to accurately detect the constantly changing bow shock boundary and thus capture its dynamic characteristics. Figure 11 shows the MHD simulated electron density and magnetic field of the bow shock image in the X-Y plane, and the location of five satellites in a single orbit for radio tomography. To test performance of the POD-based reconstruction method, we select six snapshots from MHD simulations at different times and at different Z-slices for the POD projection. The mean square errors committed by the proposed OPR technique and the regularized direct method introduced by *Zhai and Cummer* [2005] are shown in Table 2. For a five-satellite tomography mission shown in Figure 12, the regularized direct method is unable to reconstruct accurately the sharp bow shock boundary, as well as the direction change of the magnetic field along the bow shock boundary. The POD-based OPR technique, however, yields a reasonably accurate reconstruction of both the bow shock boundary and the magnetic field direction as shown in Figure 13. If two more snapshots selected from the MHD simulations

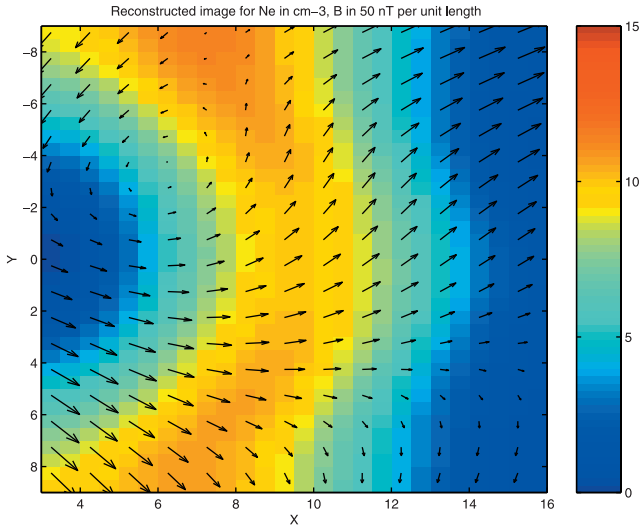

Figure 12. The reconstruction from regularized direct method for a five-satellite radio tomography mission.

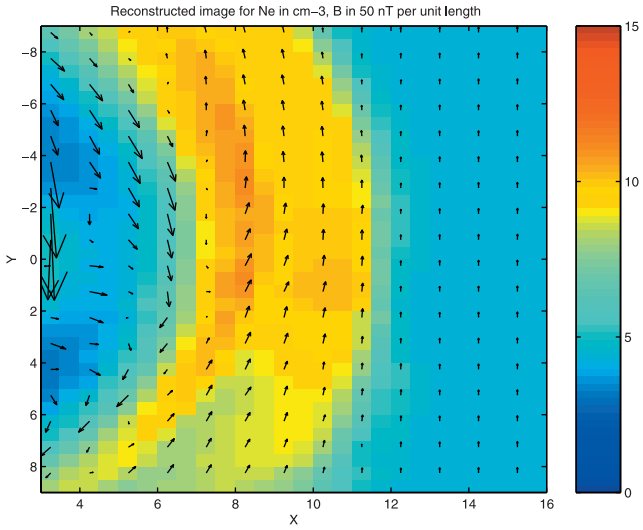

Figure 13. The six-snapshot POD-based reconstructions for a five-satellite radio tomography mission.

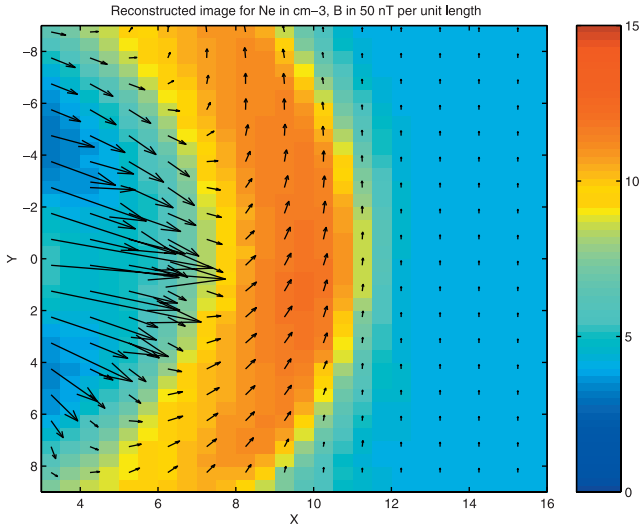

Figure 14. The eight-snapshot POD-based reconstructions for a five-satellite radio tomography mission.

at different Z-slices are added into the POD-based reconstruction, a significant improvement is achieved as shown in Table 2 and Figure 14. Table 3 shows the mean square error percentages between each snapshot selected for POD projection and the true image reconstructed.

[30] The large mean square errors of B_x or B_y committed by the reconstruction without additional information are mainly due to turbulence of the magnetic field in the probed region as shown in the MHD simulations in Figure 11 on the left side of the image. The POD-based method, when incorporating additional information from snapshots not very close to the true image, however, can still improve the reconstruction compared to the regularized direct method. This demonstrates again flexibility and robustness of the POD-based reconstruction method.

[31] Accuracy of the POD-based reconstruction depends not only on the number of total POMs used for projection but also on inconsistency of snapshots used to extract these representative POMs. Including more snapshots that are too far from the true image may degrade performance of OPR method. On the other hand, including more linearly independent snapshots whose line-of-sight projections are consistent with the measurements will lead to a more accurate reconstruction. For instance, for the bow-shock example with six snapshots, the mean-square errors of the projected TEC measurements of the six snapshots with true measurements used in the bow-shock example are 21% and 150%; the mean-square errors of the projected Faraday rotations of the six snapshots with true measurements are 270% and 350%. We note that the POD-based reconstruction works well as shown in Table 2 for snapshots whose mean-square errors of the projections with true measurements are not greater than these values.

[32] With snapshots obtained from either prior models or past experiments, the smoothing parameters λ_1 and λ_2 in the direct regularization in (4) should be determined based not only on the regularization scheme as discussed by *Zhai and Cummer* [2005] but also on the overall smoothness of these snapshots. How to quantify the selection of λ_1 and λ_2 for an optimal POD-based reconstruction requires further investigation.

4. Limitations and Discussions

[33] One limitation of the direct method with deterministic regularization is its tendency to overly smooth sharp gradients [*Kamalabadi et al.*, 2002; *Zhai and Cummer*, 2005] such as the bow shock location in the probed regions, particularly in the reconstruction of the vector magnetic field. In situations where the solution is not globally smooth, the POD-based OPR method incorporates easily additional information into the direct reconstruction via an orthogonal projection and thus can improve significantly the reconstruction. However, in situations where little statistical information is available, i.e., only few snapshots ($\leq$5) can be used for extracting the POMs, the reconstruction depends on how far are the snapshots obtained from either numerical models or past measurements to the true image. The reconstruction errors committed by the POD-based method can be worse if the snapshots are too far away from the the true image. The strategy is, depending on situations, we either collect as many useful snapshots as possible in the case of not too sparse line-of-sight measurements; or select just a few snapshots whose line-of-sight projections are consistent with the path-integrated measurements for the POD projection in the case of sparse measurements.

[34] In practice, we do not known the true image of the probed region. Therefore the challenges for a tomographic imaging are, how many snapshots should we use for the POD projection and which snapshot should we select if we are not sure how different are the snapshots from the true image? We suggest a two-step predictor-corrector strategy that may be applied as follows: First, perform a direct reconstruction with regularization and calculate the distance (mean square error norm) between the reconstructed image and each available snapshot; then remove snapshots that are too far from the reconstructed image, i.e., snapshots having mean square errors with the reconstructed image greater than 60% should not be used, and perform the POD-based reconstruction with OPR. The direct reconstruction with regularization represents agreement with the path-integrated measurements. The rational of the two-step strategy is that we select snapshots that best agree with the path-integrated measurements for the POD-based reconstruction. An advantage of this method is that the final reconstruction may agree considerably well with both the path-integrated measurements, and the prior information of the solution in the snapshots selected. An alternative but more direct way of imposing agreement with measurements is to remove snap-

Table 3. Mean Square Error Percentages Between the Selected Snapshots and the True X-Y Plane Bow Shock Image to Be Reconstructed[a]

	Snapshot Number							
Parameters	1	2	3	4	5	6	7	8
N_e	26.5	26.7	26.6	166	161	159	4.35	7.75
B_x	97.4	24.5	24.8	98.1	15.9	16.0	107	29.0
B_y	264	230	238	138	48.3	76.3	150	119

[a]The errors committed by POD-based reconstruction are given in Table 2.

shots whose line-of-sight projections are too far from the path-integrated measurements. The POD-based reconstruction is better than the regularized direct reconstruction because it uses snapshots whose projection is maximally consistent with the path-integrated measurements. The reconstruction agrees best with the measurements and contains a priori information of the solution.

[35] The projection of path-integrated equations onto the subspace spanned by a few empirical POMs may remove some details of the original images due to radical truncations in the POD as reported in the earlier applications of POD to turbulence [*Holmes et al.*, 1996]. However, in its application to magnetospheric radio tomography, the combination of POMs with path-integrated measurements may eliminate, or at least compensate for, such a problem. The prior information for the POD projection must be used with care to avoid overwhelming the information contained in measured data. Although the proposed OPR technique can significantly improve conditioning of the inverse problem, the reconstructed solution is nonunique in that it strongly depends on the empirical model where snapshots are generated, and the improvement of the reconstruction is only as good as the a priori information that is consistent with the measurements. One should be careful about unphysical improvement over the sampling theorem.

[36] We demonstrate here an orthogonal projection-based reconstruction for problems that are stationary in time. The magnetospheric structures and boundaries such as the bow shock and the plasma sheet are ever changing with solar wind conditions and geomagnetic activity; their location and orientation may be constrained by the geometry of the solar wind. The generalization of the proposed POD-based reconstruction to problems with time-varying magnetospheric parameters will be addressed in our future work.

5. Conclusions

[37] We introduce an orthogonal projection-based reconstruction (OPR) technique for radio tomographic imaging of the Earth's magnetosphere. Numerical simulations based on MHD model magnetospheric parameters and hypothetical satellite constellations were presented, and we showed that statistical model information that has been gathered from numerical models or past measurements can be easily incorporated into the direct reconstruction techniques. In this algorithm, the line-of-sight equations are projected onto the subspace spanned by an orthonormal basis extracted from an ensemble of snapshots. These snapshots represent prior knowledge of the solution, whose inclusions may considerably improve the reconstruction. Most importantly, this algorithm is robust and reasonably accurate even when relatively few satellites (4–6) are used for the reconstruction of magnetospheric regions with sharp density and field distribution. In the framework of this approach it is easy to control the tradeoff between enforcing agreement with the path-integrated measurements, statistical information, and overall smoothness of the image. Simulations show that this technique gives good results in dramatically different regions (i.e., the plasma sheet and the bow shock) of the magnetosphere with a few number of snapshots. Even with sparse path-integrated measurements, which may be imposed by the realities of satellite missions, radio tomography should enable the large-scale measurements needed to resolve many open questions in magnetospheric physics.

[38] **Acknowledgments.** This research was supported by NASA Geospace Sciences grant NAG5-12072.

[39] Arthur Richmond thanks Farzad Kamalabadi and another reviewer for their assistance in evaluating this paper.

References

Austen, J. R., S. J. Franke, and C. H. Liu (1988), Ionospheric imaging using computerized tomography, *Radio Sci.*, *23*(3), 299–307.

Castrillo, J. E., and K. Amaratunga (2002), Fast estimation of continuous Karhunen-Loève eigenfunctions using wavelets, *IEEE Trans. Signal Proc.*, *50*(1), 78–86.

Cummer, S., M. Reiner, B. Reinisch, M. Kaiser, J. Green, R. Benson, R. Manning, and K. Goetz (2001), A test of magnetospheric radio tomographic imaging with image and wind, *Geophys. Res. Lett.*, *28*(6), 1131–1134.

Cummer, S., et al. (2003), Advances in magnetospheric radio wave analysis and tomography, *Adv. Space Res.*, *32*(3), 329–336.

Demoment, G. (1989), Image reconstruction and restoration: Overview of common estimation structures and problems, *IEEE Trans. Acoust. Speech Signal Proc.*, *37*(12), 2024–2036.

DeZeeuw, D. L., T. Gombosi, C. P. T. Groth, K. G. Powell, and Q. F. Stout (2000), An adaptive MHD method for global space weather simulations, *IEEE Trans. Plasma Sci.*, *28*(6), 1956–1965.

Ergun, R., et al. (2000), Feasibility of a multisatellite investigation of the earth's magnetosphere with radio tomography, *J. Geophys. Res.*, *105*(A7), 361–373.

Fougere, P. (1995), Ionospheric radio tomography using maximum entropy: 1. Theory and simulation studies, *Radio Sci.*, *30*(2), 429–444.

Ganguly, S., G. Bavel, and A. Brown (2000), Imaging electron density and magnetic field distributions in the magnetosphere: A new technique, *J. Geophys. Res.*, *105*(A7), 16,063–16,081.

Hastie, T., R. Tibshirani, and J. Friedman (2001), *The Elements of Statistical Learning*, Springer, New York.

Holmes, P., J. L. Lumley, and G. Berkooz (1996), *Turbulence, Coherent Structures, Dynamical Systems and Symmetry*, Cambridge Univ. Press, New York.

Hung, E. S., and S. D. Senturia (1999), Generating efficient dynamical models for microelectromechanical systems from a few finite-element simulation runs, *IEEE J. Microelectromech. Syst.*, *8*(3), 280–289.

Kamalabadi, F., W. Karl, J. Semeter, D. Cotton, T. Cook, and S. Chakrabarti (1999), A statistical framework for space-based EUV ionospheric tomography, *Radio Sci.*, *34*(2), 437–447.

Kamalabadi, F., et al. (2002), Tomographic studies of aeronomic phenomena using radio and uv techniques, *J. Atmos. Sol. Terr. Phys.*, *64*, 1573–1580.

Kunitsyn, V. E., and E. D. Tereshchenko (2003), *Ionospheric Tomography*, Springer, New York.

Lin, T., and M. Pourahadi (1998), Nonparametric and non-linear models and data mining in time series: A case-study on the Canadian lynx data, *Appl. Stat.*, *47*(2), 187–201.

Loève, M. (1955), *Probability Theory*, Van Nostrand, New York.

Moore, B. (1981), Principal component analysis in linear systems: controllability, observability, and model reduction, *IEEE Trans. Auto. Control*, *26*(1), 17–32.

Muller, N., L. Magaia, and B. M. Herbst (2004), Singular value decomposition, eigenfaces, and 3D reconstructions, *SIAM Rev.*, *46*(3), 518–545.

Raymund, T. D., Y. Bresler, D. N. Anderson, and R. E. Daniell (1994), Model-assisted ionospheric tomography: A new algorithm, *Radio Sci.*, *29*(6), 1493–1512.

Sutton, E., and H. Na (1996), Ionospheric tomography using the residual correction method, *Radio Sci.*, *31*(3), 489–496.

Walker, I., J. Heaton, L. Kersley, C. Mitchel, S. Pryse, and M. Williams (1996), Eiscat verification in the development of ionospheric tomography, *Ann. Geophys.*, *14*, 1413–1421.

Zhai, Y. (2003), Model-order reduction for efficient simulation of nonlinear electro-magneto-thermal coupled problems, Ph.D. thesis, Univ. of Fla., Gainesville, Fla.

Zhai, Y., and S. A. Cummer (2005), A flexible and robust direct reconstruction method for magnetospheric radio tomography, *Radio Sci.*, *40*, RS3004, doi:10.1029/2004RS003100.

S. A. Cummer and Y. Zhai, Electrical and Computer Engineering Department, Duke University, Box 90291, Durham, NC 27708, USA. (cummer@ee.duke.edu; zhaiyh@ee.duke.edu)